ACS APPLIED MATERIALS & INTERFACES

Research Article

www.acsami.org

Porous Nickel Hydroxide–Manganese Dioxide-Reduced Graphene Oxide Ternary Hybrid Spheres as Excellent Supercapacitor Electrode Materials

Hao Chen,[†,‡] Shuxue Zhou,[†] and Limin Wu*[,†]

[†]Department of Materials Science and Advanced Materials Laboratory, Fudan University, Shanghai 20043, PR China

[‡]School of Engineering, and National Engineering and Technology Research Center of Wood-based Resources Comprehensive Utilization, Zhejiang Agriculture and Forestry Unversity, Hangzhou Lin'an 311300, PR China

Supporting Information

ABSTRACT: This paper reports the first nickel hydroxide–manganese dioxide–reduced graphene oxide ($Ni(OH)_2$-MnO_2-RGO) ternary hybrid sphere powders as supercapacitor electrode materials. Due to the abundant porous nanostructure, relatively high specific surface area, well-defined spherical morphology, and the synergetic effect of $Ni(OH)_2$, MnO_2, and RGO, the electrodes with the as-obtained $Ni(OH)_2$-MnO_2-RGO ternary hybrid spheres as active materials exhibited significantly enhanced specific capacitance (1985 $F{\cdot}g^{-1}$) and energy density (54.0 $Wh{\cdot}kg^{-1}$), based on the total mass of active materials. In addition, the $Ni(OH)_2$-MnO_2-RGO hybrid spheres-based asymmetric supercapacitor also showed satisfying energy density and electrochemical cycling stability.

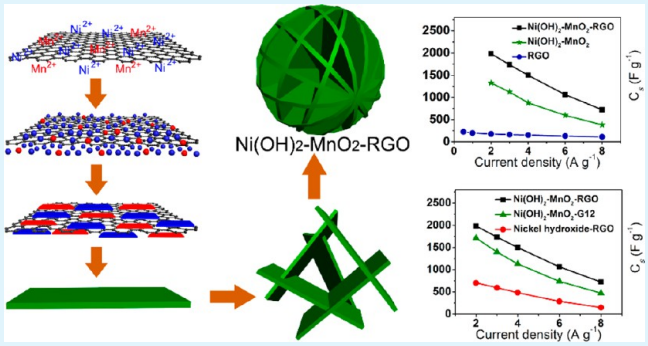

KEYWORDS: *graphene, manganese dioxide, nickel hydroxide, ternary hybrid spheres, supercapacitor*

INTRODUCTION

Supercapacitors, also known as electrochemical capacitors, have been widely applied in the fields of vehicles (especially electric vehicles, hybrid vehicles, and special heavy-duty vehicles), electric power, railways, telecommunications, and consumer electronics products.[1−3] As the main contributors of electrical energy storage of supercapacitors, electrode materials are considered to be the current research focus in the energy storage field. In particular, the pseudocapacitive electrode materials based on transitional metal oxides and hydroxides have attracted increasing interest in recent years,[4−10] because they have larger energy densities and specific capacitances with fast, reversible faradaic reactions, by at least 1 order of magnitude higher than those of carbon-based electrochemical double layer capacitors.[1,11] However, due to their low specific surface area, or inappropriate (too high or too low) crystallinity, or poor electrolyte wettability, or weak electron transportation ability, lots of transitional metal oxides and hydroxides do not give full play to their capacitance performance.[12] Therefore, how to improve the electrolyte access and electron transportation by reasonably designing structure and composition becomes the key strategy to develop high performance metal oxide/hydroxide pseudocapacitive materials.

It is well-known that nickel- and manganese-based oxides/hydroxides possess high theoretic specific capacitance, low cost, abundant sources, and environmentally friendly nature.[3,13−16] For example, Ozkan et al. fabricated a MnO_2 nanowire based hybrid nanostructured foam, which exhibited excellent specific capacitance (1109 F g^{-1}).[17] Dai et al. reported a $Ni(OH)_2$ based hybrid material as the electrode with very high specific capacitance of 1335 F g^{-1}.[18] Very recently, we have reported a novel one-step method for synthesizing $Ni(OH)_2$-MnO_2 hybrid nanosheets.[19] The as-prepared hybrid nanosheets *in situ*-supported on nickel foam as a supercapacitor electrode exhibited ultrahigh specific capacitance (C_s, 2628 $F{\cdot}g^{-1}$ at 3 $A{\cdot}g^{-1}$). However, most of this related research focuses on the nickel- and manganese-based oxides/hydroxides binary composites as electrode materials to date; little involves nickel–manganese–graphene based ternary hybrid structures for supercapacitors. In this study, we successfully synthesize the first nickel hydroxide–manganese dioxide–reduced graphene oxide ($Ni(OH)_2$-MnO_2-RGO) ternary hybrid sphere powders, through a one-step hydrothermal codeposition of graphene oxide (GO) and the precursors of nickel hydroxide and manganese dioxide. Benefitting from the abundantly porous nanostructure, relatively high specific surface area, well-defined spherical morphology, and the synergetic effect of $Ni(OH)_2$, MnO_2, and RGO, these novel $Ni(OH)_2$-MnO_2-RGO ternary hybrid spheres as the supercapacitor electrode material exhibit significantly enhanced specific capacitance (1985 $F{\cdot}g^{-1}$) and

Received: March 11, 2014
Accepted: May 5, 2014
Published: May 5, 2014

   dx.doi.org/10.1021/am5014375 | ACS Appl. Mater. Interfaces 2014, 6, 8621−8630

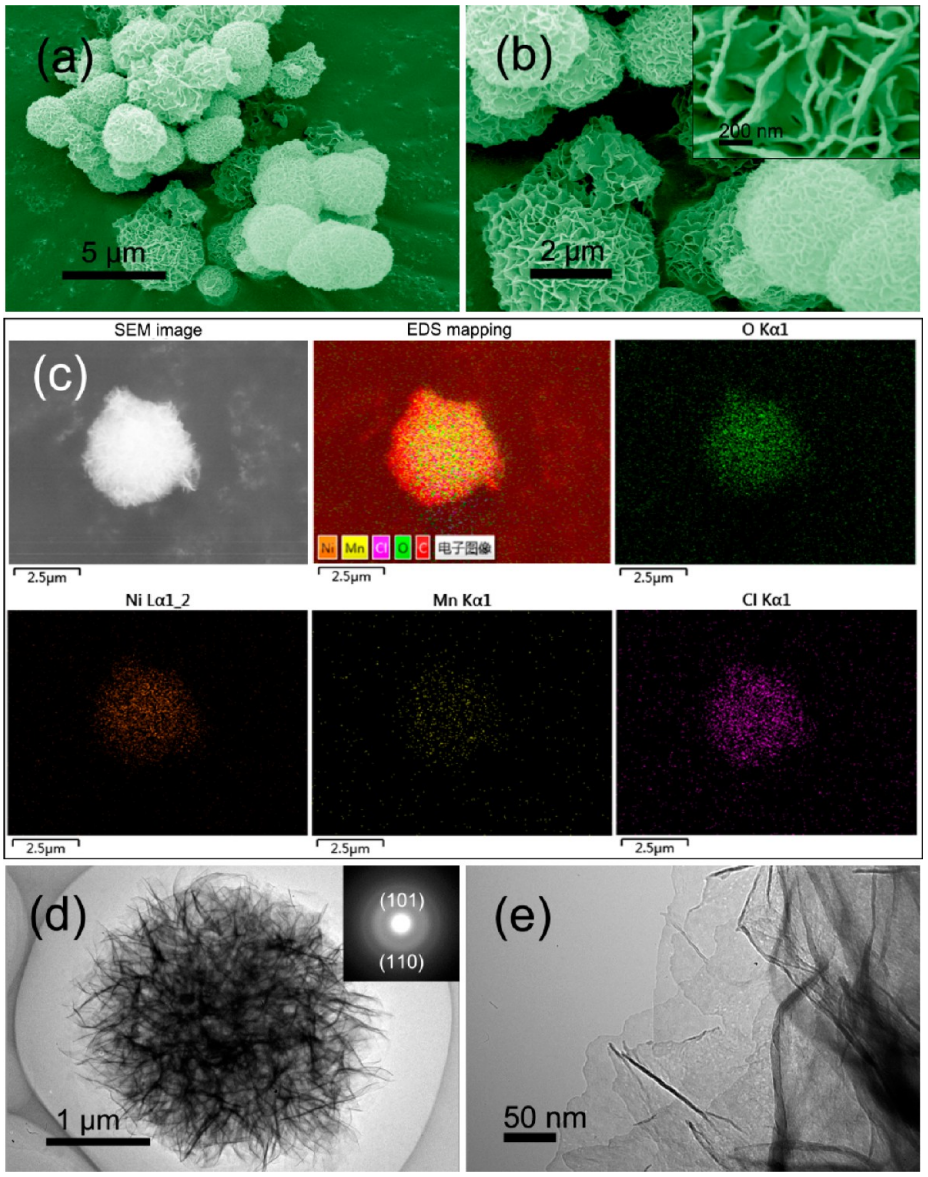

Figure 1. Typical SEM images of (a) the $Ni(OH)_2$-MnO_2-RGO hybrid spheres and (b) the hybrid spheres at higher magnification, in which the inset is the image of hybrid nanosheets. (c) SEM elemental mappings of the hybrid sphere. Typical TEM images of (d) the hybrid sphere (the inset is the SAED pattern of the whole hybrid sphere) and (e) a typical sphere edge at higher magnification (GO suspension: 0.20 g).

energy density (54.0 $Wh \cdot kg^{-1}$), based on the total mass of active materials. These values are obviously higher than those of most previously reported nickel−manganese oxide/hydroxide, manganese dioxide−graphene, nickel oxide/hydroxide−graphene, and typical nickel−cobalt binary oxide/hydroxide−graphene composites. In addition, the $Ni(OH)_2$-MnO_2-RGO ternary hybrid sphere-based asymmetric supercapacitor with porous freeze-dried RGO as the negative electrode material also exhibits satisfying energy density and electrochemical cycling stability.

EXPERIMENTAL SECTION

Materials. Hydrochloric acid (37%, HCl) was purchased from Shanghai Chemical Reagent Co., Ltd. (China). Potassium hydroxide (KOH), nickel nitrate ($Ni(NO_3)_2 \cdot 6H_2O$), manganese chloride ($MnCl_2 \cdot 4H_2O$), acetone, anhydrous ethanol, and methanol were purchased from Sinopharm Chemical Reagent Corp (China). Acetylene black (F-900, AB) was purchased from Tianjin Ebory Chemical Co., Ltd. (China). All reagents were used as received. Graphene oxide (GO) was prepared by our previously reported method.[20] Cationic gemini surfactant G12 ($C_{12}H_{25}N(CH_3)_2(CH_2)_6(CH_3)_2NC_{12}H_{25}Br_2$) was synthesized according to our previous report.[19]

Synthesis of Hybrid Materials. The $Ni(OH)_2$-MnO_2-RGO hybrid material was prepared by a simple one-step process as follows: Typically, a solution of $Ni(NO_3)_2 \cdot 6H_2O$ (0.34 mmol), $MnCl_2 \cdot 4H_2O$ (0.51 mmol), and methanol (4.0 g) was slowly added into the magnetically stirred homogeneous suspension containing GO aqueous suspension (0.20 g, 1.44 wt %), H_2O (3.0 g), and methanol (8.0 g). The as-obtained suspension was transferred to a 100 mL Teflon autoclave. The autoclave was then sealed and kept at 180 °C for 24 h to allow the growth of $Ni(OH)_2$-MnO_2-RGO hybrid material, through the following reactions: (i) methanol and NO_3^- undergo a redox reaction releasing hydroxyl ions under 180 °C: $4CH_3OH + NO_3^- \rightarrow 4HCHO + NH_3 + OH^- + 2H_2O$;[21,22] (ii) the Ni^{2+}

dx.doi.org/10.1021/am5014375 | ACS Appl. Mater. Interfaces 2014, 6, 8621−8630

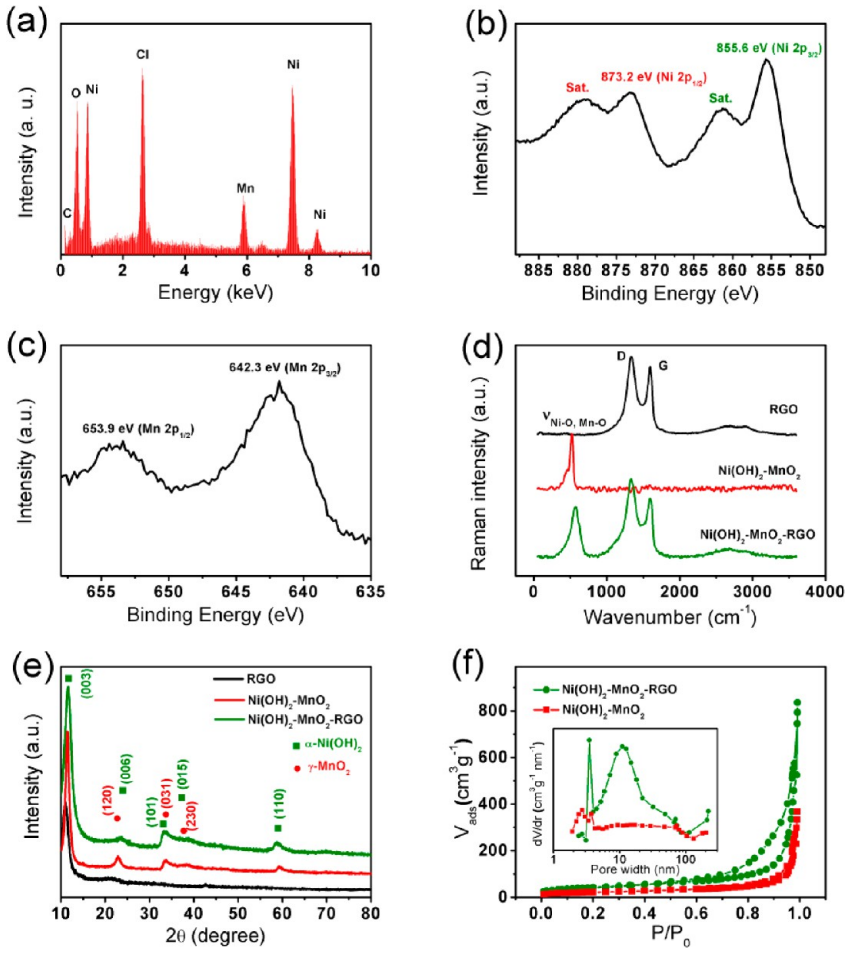

Figure 2. (a) EDX spectrum of hybrid spheres. (b) Ni 2p and (c) Mn 2p XPS scans of the hybrid spheres. (d) Raman spectra and (e) XRD patterns of RGO, $Ni(OH)_2$-MnO_2, and $Ni(OH)_2$-MnO_2-RGO powders. (f) Nitrogen (77 K) adsorption/desorption isotherms and BJH pore size distribution of as-synthesized $Ni(OH)_2$-MnO_2 and $Ni(OH)_2$-MnO_2-RGO powders.

ions from the $Ni(NO_3)_2$ solution and Mn^{2+} ions from the $MnCl_2$ solution react with OH^- ions to form $Ni(OH)_2$ and $Mn(OH)_2$; and (iii) the $Mn(OH)_2$ converts to stable MnO_2 upon reaction with oxygen. GO is reduced to RGO by reacting with methanol at high temperatures.[23] After being cooled to room temperature, the resultant product was centrifuged and washed with H_2O and ethanol several times to remove surface ions and molecules, followed by being dried at 80 °C for 12 h to remove the adsorbed solvents. For the sake of comparison, the hybrid materials with surfactant G12 to replace RGO, or without using Mn^{2+}, or different GO feeding amounts (the total water amount was kept at 3.20 g) were also fabricated using the same procedure.

Fabrication of Electrodes. Nickel foam was first pretreated successively with acetone, 2 M HCl solution, absolute ethanol, and deionized water, each for 15 min, to ensure a clean surface. The freeze-dried reduced graphene oxide (FRGO) was produced according to our previous report.[19] Hybrid- and FRGO-electrodes were fabricated as follows: a mixture of hybrid (or FRGO) powders, 23 wt % of acetylene black (as the electrical conductor), 5 wt % of polytetrafluorene−ethylene (as the binder), and a small amount of water was prepared by milling to produce a homogeneous paste. This paste was then pressed onto nickel foam current-collectors to produce hybrid and FRGO electrodes. The loading densities of active materials were about 6 mg·cm^{-2} for all electrodes.

Characterization. The morphologies were observed by scanning electron microscopy (SEM, S-4800, Hitachi), and the TEM images were obtained on a Philips CM200FEG field emission microscope. The crystalline structure was characterized by XRD patterns recorded in a Rigaku D/max-kA diffractometer with Cu Kα radiation. X-ray photoelectron spectroscopy (XPS, PHI 5000C ESCA System), energy-dispersive X-ray spectroscopy (EDX, TSL, AMETEK), and Raman spectroscopy (Jobin Yvon LabRam-1B) measurements were employed to investigate the compositions of the samples. An automated adsorption apparatus (Micromeritics, ASAP 2010) was used to analyze the surface characteristics of the samples using gas physisorption at 77 K.

Electrochemical Measurement. The electrochemical properties of the as-obtained hybrid powder- and the FRGO-based electrodes were investigated under a three-electrode cell configuration at 25 °C in 1 M KOH. The electrodes were soaked in a 1 M KOH solution and degassed in a vacuum for 5 h before the electrochemical test. Platinum foil and a saturated calomel electrode (SCE) were used as the counter and reference electrodes, respectively. The electrochemical properties of the asymmetric supercapacitor were investigated under a two-electrode cell configuration with $Ni(OH)_2$-MnO_2-RGO hybrid powder as the positive electrode material and FRGO as the negative electrode material in 1 M KOH electrolyte solution. The cyclic voltammetry (CV), galvanostatic charge−

dx.doi.org/10.1021/am5014375 | ACS Appl. Mater. Interfaces 2014, 6, 8621−8630

Scheme 1. Possible Formation Mechanism of $Ni(OH)_2$-MnO_2-RGO Hybrid Sphere and the Structural Schematic Diagram of a Single Nanosheet in a Hybrid Sphere

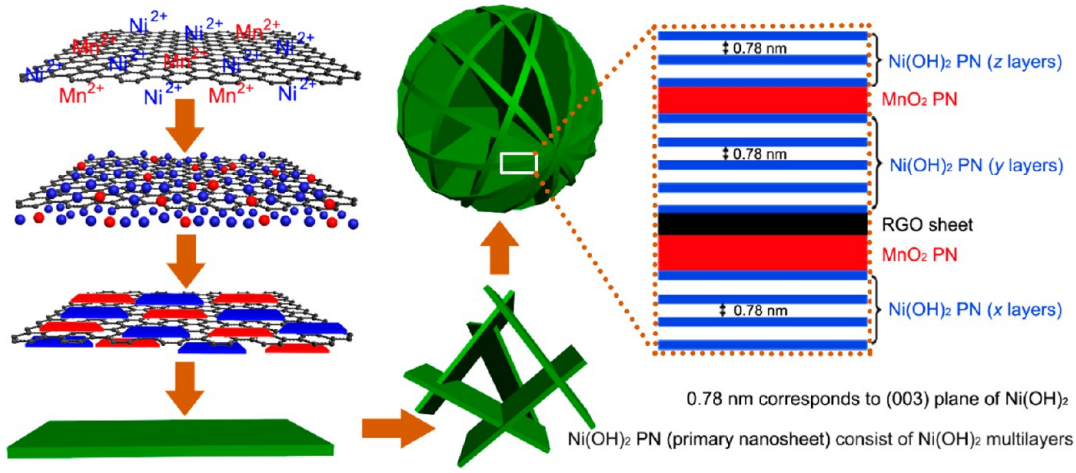

discharge, and electrochemical impedance spectroscopy (EIS) measurements were conducted on a CHI 660E electrochemical workstation (Shanghai CH Instrument Company, China).

RESULTS AND DISCUSSION

Morphology and Composition of Hybrid Spheres. The typical SEM image of the as-obtained hybrid powders, as shown in Figure 1a, presents a spherical feature with diameters of 1−5 μm, and these hybrid spheres possess a porous flowerlike hierarchical structure composed of nanosheets with dozens of nanometers thick (Figure 1b). This hierarchical structure facilitates the charge transport and ion diffusion. SEM elemental mappings (Figure 1c) reveal a uniform distribution of Ni, Mn, O, and Cl elements in the as-obtained sphere (the existence of C element cannot be determined due to the effect of carbon conductive adhesive). This indicates a relatively uniform chemical composition of the as-obtained hybrid sphere. The TEM images of the as-obtained hybrid sphere further display a rough and transparent edge (Figure 1d), indicating an ultrathin nature. The selected-area electron diffraction (SAED) pattern of the hybrid sphere reveals two well-defined diffraction rings (inset of Figure 1d), suggesting its polycrystalline nature. The energy-dispersive X-ray (EDX) spectra of the entire area and center area of the hybrid sphere (Figure S1a and b in the Supporting Information) show the similar element composition of Ni, Mn, O, Cl, and C elements, except for the Cu signal from the Cu grid. A higher-magnification TEM image of a typical sphere edge clearly shows that this hybrid sphere consists of ultrathin nanosheets, which are composed of several thinner layers (Figure 1e). The EDX spectrum of the edge region of the hybrid sphere (Figure S1c) suggests that these thinner layers may be the stacked structure of $Ni(OH)_2$, MnO_2, and graphene layers (the absence of Cl element may be attributed to the ion migration of Cl^-).

The EDX spectrum (Figure 2a) and the full XPS spectrum (Figure S 1d) of the as-prepared hybrid powder sample further prove the basic element composition of as-obtained spheres, Ni, Mn, O, C, and Cl elements, which should be contributed by the composition of $Ni(OH)_2$, MnO_2, and RGO. The Ni 2p XPS spectrum is found to have two shakeup satellites (indicated as "Sat") close to two spin−orbit doublets at 873.2 and 855.6 eV (Figure 2b). These are here given as Ni $2p_{1/2}$ and Ni $2p_{3/2}$ signals of $Ni(OH)_2$, respectively.[24,25] The Mn 2p XPS spectrum displays two characteristic peaks at 642.3 and 653.9 eV, corresponding to the Mn $2p_{3/2}$ and Mn $2p_{1/2}$ spin−orbit peaks of MnO_2 (Figure 2c), confirming the existence of $Ni(OH)_2$ and MnO_2 in the hybrid spheres.[26,27] The XPS scan of pure RGO prepared by a similar hydrothermal process showed a decreasing O/C ratio from 0.38 to 0.23 (Figure S1e), and its Raman spectrum demonstrated an increasing D/G band intensity ratio from 1.07 to 1.15 (Figure S1f) after the hydrothermal reaction. These results indicate that GO has been reduced to RGO by this hydrothermal treatment.[28,29] Moreover, the comparison of C 1s XPS spectra of GO and RGO further revealed that the decrease of the O/C ratio was mainly caused by the proportional reduction of ester and carbonyl groups (Figure S1g).

The Raman spectrum of hybrid sphere powders displays a D band at 1335 cm^{-1}, a G band at 1585 cm^{-1} for RGO, and another band from 540 to 670 cm^{-1} for the Ni−O and Mn−O stretching vibrations of $Ni(OH)_2$ and MnO_2 (Figure 2d).[30,31] The XRD patterns show that the well-defined diffraction peaks of $Ni(OH)_2$-MnO_2-RGO can be successfully indexed to the α-$Ni(OH)_2$ phase (JCPDS 38-0715), γ-MnO_2 phase (JCPDS 14-0644), and the AB stacking order of graphene sheets (10.4°, corresponding to interlayer spacing of 0.85 nm, Figure 2e),[29] which is similar to that of our previously reported $Ni(OH)_2$-MnO_2 hybrid nanosheets.[19] The as-obtained hybrid sphere powder appeared black, different from the brown color of $Ni(OH)_2$-MnO_2 binary powder (Figure S1h). These results indicate that the as-obtained hybrid spheres are composed of α-$Ni(OH)_2$, γ-MnO_2, and RGO, and the Cl^- ions may act as the intercalated counteranions of layered α-$Ni(OH)_2$ based on the above EDX result. In addition, the $Ni(OH)_2$-MnO_2-RGO ternary hybrid sphere has the BET and Langmuir surface areas of 147 and 185 $m^2\ g^{-1}$, respectively, which are almost double those of the $Ni(OH)_2$-MnO_2 (76 and 96 $m^2\ g^{-1}$, respectively), as indicated by Figure 2f.

Possible Formation Mechanism of Hybrid Spheres. The similar diffraction peaks between $Ni(OH)_2$-MnO_2-RGO and $Ni(OH)_2$-MnO_2, as shown in the XRD pattern (Figure 2e), suggest that the nanosheets in hybrid spheres form through a mechanism similar to the preferentially oriented growth of $Ni(OH)_2$ nanosheets described in previous reports.[19,32,33] As shown in Scheme 1, due to the electrostatic interaction, most Ni^{2+} and Mn^{2+} ions are located on the surfaces of GO sheets

dx.doi.org/10.1021/am5014375 | ACS Appl. Mater. Interfaces 2014, 6, 8621−8630

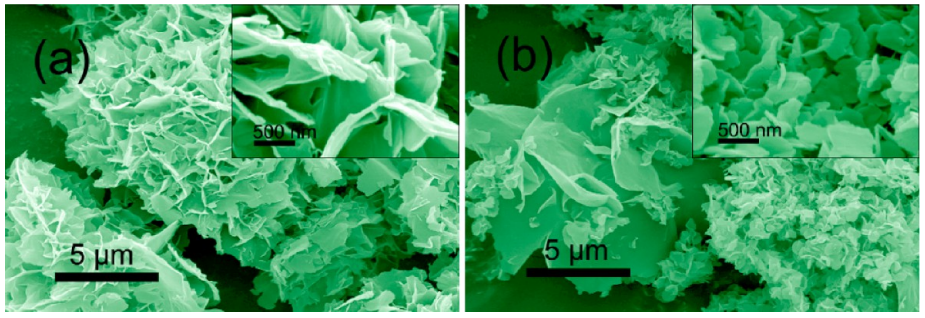

Figure 3. SEM images of the (a) $Ni(OH)_2$-MnO_2-G12 and (b) nickel hydroxide−RGO powders.

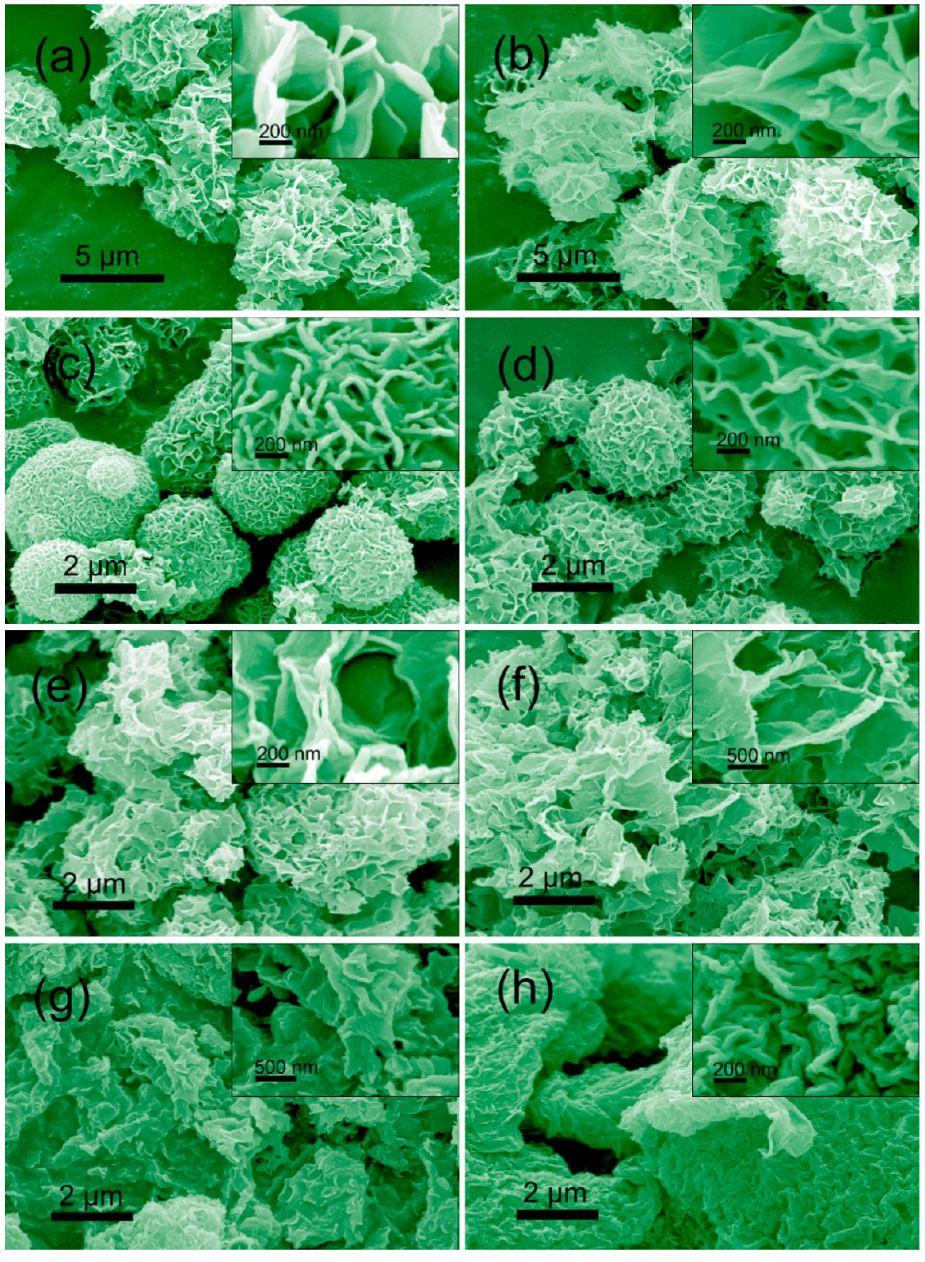

Figure 4. SEM images of the $Ni(OH)_2$-MnO_2-RGO powders with different GO suspension amounts: (a) 0.00, (b) 0.05, (c) 0.10, (d) 0.40, (e) 0.60, (f) 0.80, and (g) 1.60 g. (h) SEM image of the pure RGO.

and first react with OH^- ions to produce primary particles. These primary particles aggregate into chains which partly deposit on the surfaces of GO to become the cores of more amorphous primary particles aggregating. As the primary particles continue to aggregate, they begin to crystallize and gradually form primary nanosheets. During this process,

dx.doi.org/10.1021/am5014375 | ACS Appl. Mater. Interfaces 2014, 6, 8621−8630

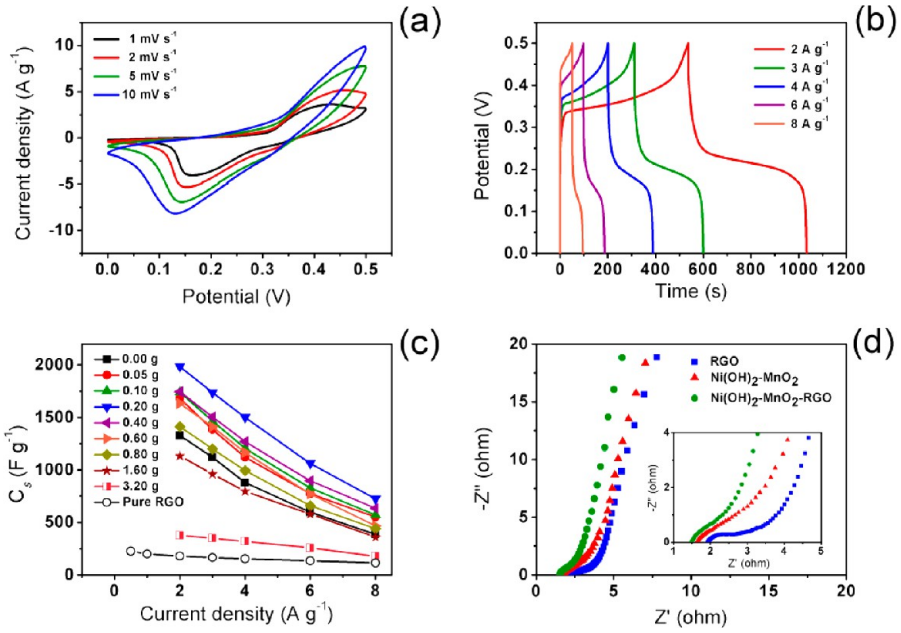

Figure 5. (a) Comparison of CV curves of $Ni(OH)_2$-MnO_2-RGO hybrid sphere-electrode at different scan rates. (b) Galvanostatic discharge curves of $Ni(OH)_2$-MnO_2-RGO hybrid sphere-electrode at different current densities. (c) Comparison of specific capacitances of the hybrid electrodes prepared with different GO amounts. (d) Comparison of Nyquist plots of $Ni(OH)_2$-MnO_2-RGO, $Ni(OH)_2$-MnO_2, and RGO electrodes.

divalent manganese is converted to tetravalent manganese by reacting with dissolved oxygen,[34,35] and GO is reduced to RGO by reacting with methanol at high temperatures.[23] Because of the hydrogen-bonding interactions between MnO_2 and $Ni(OH)_2$ primary nanosheets, MnO_2 primary nanosheets may disorderly stack with $Ni(OH)_2$ primary nanosheets and grow along with RGO to form a hybrid nanosheet (Scheme 1). These nanosheets tend to aggregate perpendicular to the surface planes to decrease the surface energy by reducing exposed areas. Therefore, as the reaction proceeds, a spontaneous energy-minimizing self-assembly of the resulting hybrid nanosheets would occur, producing spherical assembled structures.[36,37] And because the intercalation of graphene sheets can weaken the excessive oriented growth and the aggregation of hybrid nanosheets, the $Ni(OH)_2$-MnO_2-RGO nanosheets finally self-assemble into a spherical shape (Figure 1a and b), rather than some irregular structures like the $Ni(OH)_2$-MnO_2 binary hybrid materials with surfactant G12 as the structure growth assisting agent (called $Ni(OH)_2$-MnO_2-G12 here, as shown in Figure 3a). And due to the too high oriented growth of pure nickel hydroxide, the nickel hydroxide-RGO without MnO_2 does not self-assemble into a spherical structure (Figure 3b). Thus, the as-obtained $Ni(OH)_2$-MnO_2-RGO ternary hybrid hierarchical structure has high surface area, a basal plane, and edge surface and may possess enhanced electrochemical properties.[38]

The Effects of GO Amounts. The GO amount also plays an important role in the morphological control of the hybrid spheres. Without GO, the as-obtained hybrid spheres consisted of relatively larger nanosheets and worse spherical structure (Figure 4a). This should be a result of the relatively high oriented growth and aggregation ability of pure $Ni(OH)_2$-MnO_2. As the GO amount increased, the assembled structures increased in size and then began to become round (Figures 4b–d and 1a,b). However, further increasing the GO amount led to the disintegration of spherical structure, and even the self-aggregation of graphene nanosheets (Figure 4e–g). This may be a result of excessive graphene wrapping the forming hybrid nanosheets and destroying their self-assembly ability. For pure RGO, due to the attractive forces between layers during the drying process,[39,40] only high aggregates were observed (Figure 4h).

Electrochemical Properties of Hybrid Sphere Electrodes. Figure 5a demonstrates the typical cyclic voltammetry (CV) curve of the as-obtained hybrid spheres, which was fabricated at a 0.20 g GO suspension feeding amount, as an electrode for a supercapacitor at different scan rates. A pair of well-defined redox peaks within 0–0.5 V can be ascribed to a faradaic redox reaction related to M–O/M–O–OC (M represents Ni or Mn, C represents H or K).[41,42] Figure 5b shows the galvanostatic charge–discharge curves of the electrode based on the as-obtained hybrid spheres at different current densities. Both indicate the strong pseudocapacitive nature of the as-obtained electrodes. The specific capacitances of the $Ni(OH)_2$-MnO_2, pure RGO, and the ternary hybrid spheres prepared at different GO feeding amounts are shown in Figure 5c. Most hybrid sphere-electrodes possess significantly higher specific capacitances than the $Ni(OH)_2$-MnO_2 or RGO electrodes. This can be attributed to the synergistic effects of the $Ni(OH)_2$-MnO_2-RGO hybrid sphere as follows: (i) The as-obtained hybrid spheres are composed of $Ni(OH)_2$-MnO_2 and RGO. Both of them can contribute their capacitance. (ii) The intercalation of graphene sheets can improve the electron transportation from hybrid sphere structures to the current collector, which can be confirmed by the decrease in equivalent series resistance (R_s, the real axis intercept), as shown in Figure 5d. (iii) The intercalation of graphene sheets can suppress the excessive self-aggregation of hybrid nanosheets and lead to visible increasing of specific surface areas as indicated by Figure 2f. This promotes better electrolyte access within the electrode materials and more efficient exposure of active sites to the electrolyte.

As the GO content increases, as shown in Figure 5c, the C_s increases. However, excessive GO, e.g., 0.40 g, decreases the C_s

dx.doi.org/10.1021/am5014375 | ACS Appl. Mater. Interfaces 2014, 6, 8621–8630

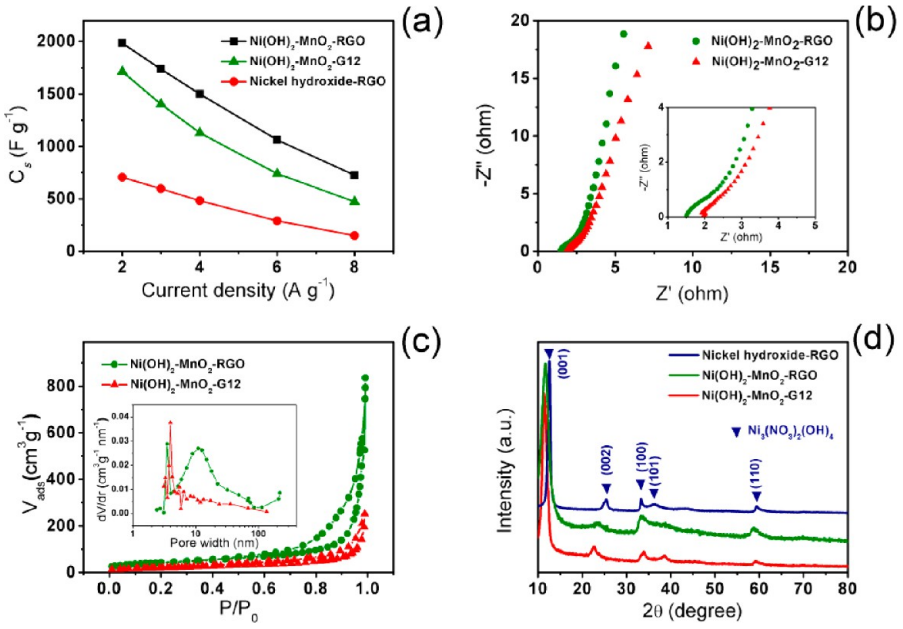

Figure 6. (a) Comparison of specific capacitances of $Ni(OH)_2$-MnO_2-RGO, $Ni(OH)_2$-MnO_2-G12, and nickel hydroxide-RGO electrodes. (b) Comparison of Nyquist plots of $Ni(OH)_2$-MnO_2-RGO and $Ni(OH)_2$-MnO_2-G12 electrodes. (c) Nitrogen (77 K) adsorption/desorption isotherms and BJH pore size distribution of as-synthesized $Ni(OH)_2$-MnO_2-G12 and $Ni(OH)_2$-MnO_2-RGO powders. (d) XRD patterns of $Ni(OH)_2$-MnO_2-RGO, $Ni(OH)_2$-MnO_2-G12, and nickel hydroxide-RGO powders.

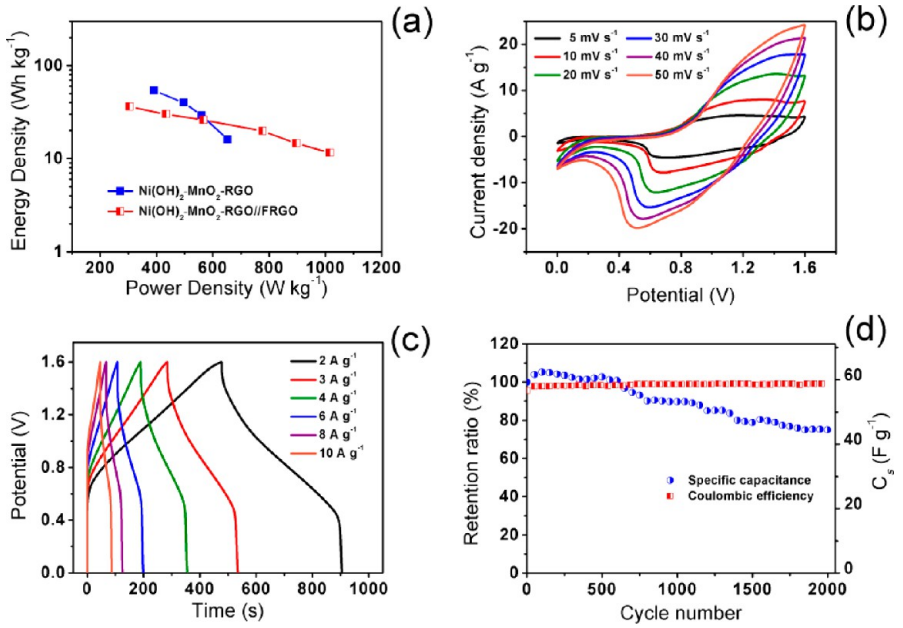

Figure 7. (a) Comparison of energy density vs power density curves of $Ni(OH)_2$-MnO_2-RGO hybrid electrode and $Ni(OH)_2$-MnO_2-RGO//FRGO asymmetric supercapacitors. (b) CV curves of the asymmetric supercapacitor at different scan rates. (c) Galvanostatic charge−discharge curves of the asymmetric supercapacitor at different current densities. (d) Cycling performance of the asymmetric supercapacitor a current density of 8 A g^{-1}.

due to the disintegration of spherical structure and the self-aggregation of graphene nanosheets as indicated by Figure 4. The excessive self-aggregation of graphene can produce higher R_s (Figure 5d), which inhibits the capacitance output. The hybrid spheres formed at 0.20 g of GO show the highest C_s values, being 1985, 1736, 1501, 1062, and 724 F·g^{-1} at current densities of 2, 3, 4, 6, and 8 A·g^{-1}, respectively. The modest decrease in C_s at higher current densities may be due to the limited ion migration into the inside of active materials, as the current density increased. This can be further improved by decreasing the loading densities of active materials. Although the rate capability is not impressive, the obtainable highest C_s (1985 F·g^{-1} at 2 A·g^{-1}) is obviously higher than the specific capacitances of most previously reported nickel−manganese oxide/hydroxide, manganese dioxide-graphene, nickel oxide/hydroxide-graphene binary, and nickel−cobalt oxide/hydroxide-graphene composites (Table S1). This high specific capacitance is believed to be caused by the unique nanostructure features of the present $Ni(OH)_2$-MnO_2-RGO hybrid spheres: (i) An abundant porous nanostructure, relatively high specific surface area, and well-defined spherical morphology allow easy electrolyte access and promote fast ion

dx.doi.org/10.1021/am5014375 | ACS Appl. Mater. Interfaces 2014, 6, 8621−8630

diffusion. (ii) The synergistic effect between $Ni(OH)_2$ and MnO_2 in hybrid spheres can improve the pseudocapacitance output of them, like our previously reported $Ni(OH)_2$-MnO_2 hybrid nanosheets.[19] (iii) The intercalation of graphene sheets improves the electron transport of binary metal oxides/hydroxides and thus enhances the synergistic effect of hybrid materials.

Figure 6a displays that the $Ni(OH)_2$-MnO_2 binary hybrid nanosheet powder ($Ni(OH)_2$-MnO_2-G12), prepared with surfactant G12 as the structure growth assisting agent, exhibits higher C_s (1402 $F{\cdot}g^{-1}$ at 3 $A{\cdot}g^{-1}$) than that of pure $Ni(OH)_2$-MnO_2 powder (1121 $F{\cdot}g^{-1}$ at 3 $A{\cdot}g^{-1}$), indicating that G12 can also improve the C_s of hybrid nanostructure powders. However, this increase is inferior to that endowed by RGO. This is because the intercalation of RGO can decrease the electric resistance and increase the specific surface area of active materials compared to G12, as shown in Figures 2f, 5d, and 6b,c.

Figure 6d demonstrates that the nickel hydroxide-RGO binary hybrid synthesized without using Mn^{2+} possesses a $Ni_3(NO_3)_2(OH)_4$ phase (JCPDS 22-0752), suggesting that the addition of GO has no influence on the crystal transition of nickel hydroxide, unlike the addition of Mn^{2+} (Figure 2e). And the nickel hydroxide-RGO has obviously lower C_s than the $Ni(OH)_2$-MnO_2-RGO ternary hybrid. These results indicate that the present ternary hybrids have better capacitance performances than binary counterparts.

On the basis of the obtainable specific capacitance values and the reported method of calculation,[43,44] the energy densities of the as-obtained $Ni(OH)_2$-MnO_2-RGO ternary hybrid sphere-electrode at 0.20 g of GO were further calculated to be 54.0, 39.9, 29.2, and 16.0 $Wh{\cdot}kg^{-1}$ at average power densities of 392, 497, 561, and 653 $W{\cdot}kg^{-1}$, respectively (Figure 7a). Although the average power densities were not impressive due to a relatively weak electric double layer capacitive nature of $Ni(OH)_2$-MnO_2-RGO, the maximum energy density (54.0 $Wh{\cdot}kg^{-1}$ at 392 $W{\cdot}kg^{-1}$) was found to exceed those of some recently reported nickel−manganese oxide/hydroxide-,[45,46] manganese dioxide-graphene-,[44,47] and nickel oxide/hydroxide-graphene-powder-based composite supercapacitor electrodes,[18,48] as shown in Table S2.

Electrochemical Properties of $Ni(OH)_2$-MnO_2-RGO//FRGO Asymmetric Supercapacitors. In order to evaluate the possibility of using the as-obtained $Ni(OH)_2$-MnO_2-RGO hybrid spheres to construct a practical supercapacitor device, we further fabricated an asymmetric supercapacitor with $Ni(OH)_2$-MnO_2-RGO hybrid spheres and porous freeze-dried reduced graphene oxide (FRGO) powders as the positive and negative electrodes materials, respectively. Figure 7b and c demonstrate that the as-fabricated $Ni(OH)_2$-MnO_2-RGO//FRGO asymmetric supercapacitor exhibits very good capacitive behavior at a potential window of 0−1.6 V. The highest energy density of the asymmetric supercapacitor can be found to be 32.6 $Wh{\cdot}kg^{-1}$ at an average power density of 305 $W{\cdot}kg^{-1}$, derived from its discharge curves. At a high power density of 1016 $W{\cdot}kg^{-1}$, the energy density can still remain at 11.5 $Wh{\cdot}kg^{-1}$ (Figure 7a). Compared with $Ni(OH)_2$-MnO_2-RGO electrode, this asymmetric supercapacitor displays a much milder attenuation in energy density due to the limitation of relatively low capacitance output of the FRGO negative electrode (281 $F{\cdot}g^{-1}$ at 0.5 $A{\cdot}g^{-1}$). However, the obtainable highest power density has a significant enhancement (Figure 7a), because of the relatively high power output nature of FRGO as electric double layer capacitive material. The obtainable highest energy density and corresponding average power density are comparable to those of some other asymmetric supercapacitors[49−53] (Table S3). We also used galvanostatic charge−discharge measurement to evaluate the capacitance durability and Coulombic efficiency of the as-fabricated asymmetric supercapacitor. As shown in Figure 7d, the as-obtained asymmetric supercapacitor can still retain about 75% of its original capacitance even after 2000 cycles, which is comparable to some nickel- and manganese-based asymmetric supercapacitors.[27,54,55] The capacitance durability can be further improved when a capsulation cell is employed to prevent the active materials from loosening or flaking off. Furthermore, it is noted that the Coulombic efficiency can be maintained at about 98% except the previous several cycles. These results demonstrate that our asymmetric supercapacitor based on $Ni(OH)_2$-MnO_2-RGO//FRGO also possesses good electrochemical stability.

CONCLUSIONS

In this work, highly porous ternary hybrid spheres composed of α-$Ni(OH)_2$, γ-MnO_2, and RGO were successfully fabricated using a facile one-step hydrothermal codeposition method. Due to the abundant porous nanostructure, relatively high specific surface area, well-defined spherical morphology, and the synergetic effects of $Ni(OH)_2$, MnO_2, and RGO, the electrodes with the as-obtained $Ni(OH)_2$-MnO_2-RGO hybrid sphere powders as active materials exhibited very high specific capacitance (1985 $F{\cdot}g^{-1}$) and energy density (54.0 $Wh{\cdot}kg^{-1}$). Both were significantly higher than those of most previously reported nickel−manganese oxide/hydroxide, manganese dioxide-graphene, nickel oxide/hydroxide-graphene binary, and typical nickel−cobalt oxide/hydroxide-graphene ternary composites. In addition, the $Ni(OH)_2$-MnO_2-RGO ternary hybrid sphere-based asymmetric supercapacitor exhibited comparable energy density and electrochemical cycling stability to some nickel- and manganese-based asymmetric supercapacitors. This suggestes that the as-prepared $Ni(OH)_2$-MnO_2-RGO ternary hybrid spheres are promising electrode materials to fabricate high performance supercapacitors by further optimized capsulation. And the present method offers a promising design and synthetic protocol of electrode materials for future supercapacitor applications.

ASSOCIATED CONTENT

Supporting Information

EDX spectra of the entire area, center area, and edge region of hybrid sphere; full XPS and C 1s XPS spectra of GO and RGO; full XPS spectra of $Ni(OH)_2$-MnO_2-RGO; Raman spectra of GO and RGO; photographs of as-obtained $Ni(OH)_2$-MnO_2 and $Ni(OH)_2$-MnO_2-RGO hybrid spheres powders. Comparison of the maximum C_s, maximum energy densities, and corresponding average power densities of some reported nickel−manganese oxide/hydroxide-, manganese dioxide-, graphene-, nickel oxide/hydroxide-graphene-, and nickel−cobalt oxide/hydroxide-graphene-based composite pseudocapacitive materials and the present work; comparison of the maximum energy densities, corresponding average power densities, and voltage range of some reported nickel or manganese oxide/hydroxide based asymmetric supercapacitors and the present work. This material is available free of charge via the Internet at http://pubs.acs.org.

AUTHOR INFORMATION

Corresponding Author

*E-mail: lmw@fudan.edu.cn.

Notes

The authors declare no competing financial interest.

ACKNOWLEDGMENTS

Financial supports were received from the National Natural Science Foundation of China (Grants 51133001 and 21374018), National "863" Foundation, Science and Technology Foundation of Ministry of Education of China (20110071130002), Science and Technology Foundation of Shanghai (12 nm0503600, 13JC1407800), Natural Science Foundation of Zhejiang Province of China (LQ14E030011), Zhejiang innovative group (2012R10023-16), BURC research foundation (2013SWZ01-2), and talents foundation (2011FR041, 2013FR066) from Zhejiang A&F University.

REFERENCES

(1) Simon, P.; Gogotsi, Y. Materials for Electrochemical Capacitors. *Nat. Mater.* **2008**, *7*, 845−854.

(2) Winter, M.; Brodd, R. J. What Are Batteries, Fuel Cells, and Supercapacitors? *Chem. Rev.* **2004**, *104*, 4245−4270.

(3) Wei, W.; Cui, X.; Chen, W.; Ivey, D. G. Manganese Oxide-Based Materials as Electrochemical Supercapacitor Electrodes. *Chem. Soc. Rev.* **2011**, *40*, 1697−1721.

(4) Cai, D.; Wang, D.; Liu, B.; Wang, Y.; Liu, Y.; Wang, L.; Li, H.; Huang, H.; Li, Q.; Wang, T. Comparison of the Electrochemical Performance of $NiMoO_4$ Nanorods and Hierarchical Nanospheres for Supercapacitor Applications. *ACS Appl. Mater. Interfaces* **2013**, *5*, 12905−12910.

(5) Vijayakumar, S.; Nagamuthu, S.; Muralidharan, G. Supercapacitor Studies on NiO Nanoflakes Synthesized Through a Microwave Route. *ACS Appl. Mater. Interfaces* **2013**, *5*, 2188−2196.

(6) Saravanakumar, B.; Purushothaman, K. K.; Muralidharan, G. Interconnected V_2O_5 Nanoporous Network for High-Performance Supercapacitors. *ACS Appl. Mater. Interfaces* **2012**, *4*, 4484−4490.

(7) Chen, H.; Zhou, S.; Chen, M.; Wu, L. Reduced Graphene Oxide-MnO_2 Hollow Sphere Hybrid Nanostructures as High-Performance Electrochemical Capacitors. *J. Mater. Chem.* **2012**, *22*, 25207−25216.

(8) Chen, H.; Hu, L.; Chen, M.; Yan, Y.; Wu, L. Nickel−Cobalt Layered Double Hydroxide Nanosheets for High-Performance Supercapacitor Electrode Materials. *Adv. Funct. Mater.* **2014**, *24*, 934−942.

(9) Wang, B.; Zhu, T.; Wu, H. B.; Xu, R.; Chen, J. S.; Lou, X. W. Porous Co_3O_4 nanowires derived from long $Co(CO_3)_{0.5}(OH)\cdot 0.11H_2O$ nanowires with improved supercapacitive properties. *Nanoscale* **2012**, *4*, 2145−2149.

(10) Wu, H. B.; Pang, H.; Lou, X. W. Facile synthesis of mesoporous $Ni_{0.3}Co_{2.7}O_4$ hierarchical structures for high-performance supercapacitors. *Energy Environ. Sci.* **2013**, *6*, 3619−3626.

(11) Inagaki, M.; Konno, H.; Tanaike, O. Carbon Materials for Electrochemical Capacitors. *J. Power Sources* **2010**, *195*, 7880−7903.

(12) Chen, M.; Ye, C.; Zhou, S.; Wu, L. Recent Advances in Applications and Performance of Inorganic Hollow Spheres in Devices. *Adv. Mater.* **2013**, *25*, 5343−5351.

(13) Liu, J.; Jiang, J.; Bosman, M.; Fan, H. J. Three-Dimensional Tubular Arrays of MnO_2-NiO Nanoflakes with High Areal Pseudocapacitance. *J. Mater. Chem.* **2012**, *22*, 2419−2426.

(14) Zhang, G.; Yu, L.; Hoster, H. E.; Lou, X. W. Synthesis of one-dimensional hierarchical NiO hollow nanostructures with enhanced supercapacitive performance. *Nanoscale* **2013**, *5*, 877−881.

(15) Wang, B.; Chen, J. S.; Wang, Z.; Madhavi, S.; Lou, X. W. Green Synthesis of NiO Nanobelts with Exceptional Pseudo-Capacitive Properties. *Adv. Energy Mater.* **2012**, *2*, 1188−1192.

(16) Ding, S.; Zhu, T.; Chen, J. S.; Wang, Z.; Yuan, C.; Lou, X. W. Controlled synthesis of hierarchical NiO nanosheet hollow spheres with enhanced supercapacitive performance. *J. Mater. Chem.* **2011**, *21*, 6602−6606.

(17) Wang, W.; Guo, S.; Bozhilov, K. N.; Yan, D.; Ozkan, M.; Ozkan, C. S. Intertwined Nanocarbon and Manganese Oxide Hybrid Foam for High-Energy Supercapacitors. *Small* **2013**, *9*, 3714−3721.

(18) Wang, H.; Casalongue, H. S.; Liang, Y.; Dai, H. $Ni(OH)_2$ Nanoplates Grown on Graphene as Advanced Electrochemical Pseudocapacitor Materials. *J. Am. Chem. Soc.* **2010**, *132*, 7472−7477.

(19) Chen, H.; Hu, L.; Yan, Y.; Che, R.; Chen, M.; Wu, L. One-Step Fabrication of Ultrathin Porous Nickel Hydroxide-Manganese Dioxide Hybrid Nanosheets for Supercapacitor Electrodes with Excellent Capacitive Performance. *Adv. Energy Mater.* **2013**, *3*, 1636−1646.

(20) Tang, Z.; Chen, H.; Chen, X.; Wu, L.; Yu, X. Graphene Oxide Based Recyclable Dehydrogenation of Ammonia Borane within a Hybrid Nanostructure. *J. Am. Chem. Soc.* **2012**, *134*, 5464−5467.

(21) Ren, Y.; Gao, L. From Three-Dimensional Flower-Like α-$Ni(OH)_2$ Nanostructures to Hierarchical Porous NiO Nanoflowers: Microwave-Assisted Fabrication and Supercapacitor Properties. *J. Am. Ceram. Soc.* **2010**, *93*, 3560−3564.

(22) Sun, X.; Qiu, X.; Li, L.; Li, G. ZnO Twin-Cones: Synthesis, Photoluminescence, and Catalytic Decomposition of Ammonium Perchlorate. *Inorg. Chem.* **2008**, *47*, 4146−4152.

(23) Dreyer, D. R.; Murali, S.; Zhu, Y.; Ruoff, R. S.; Bielawski, C. W. Reduction of Graphite Oxide Using Alcohols. *J. Mater. Chem.* **2011**, *21*, 3443−3447.

(24) Lee, J. W.; Ahn, T.; Soundararajan, D.; Ko, J. M.; Kim, J.-D. Non-Aqueous Approach to the Preparation of Reduced Graphene Oxide/α-$Ni(OH)_2$ Hybrid Composites and Their High Capacitance Behavior. *Chem. Commun.* **2011**, *47*, 6305−6307.

(25) McIntyre, N. S.; Cook, M. G. X-ray Photoelectron Studies on Some Oxides and Hydroxides of Cobalt, Nickel, and Copper. *Anal. Chem.* **1975**, *47*, 2208−2213.

(26) Xiong, Y.; Xie, Y.; Li, Z.; Wu, C. Growth of Well-Aligned γ-MnO_2 Monocrystalline Nanowires through a Coordination-Polymer-Precursor Route. *Chem.—Eur. J.* **2003**, *9*, 1645−1651.

(27) Wu, Z. S.; Ren, W.; Wang, D. W.; Li, F.; Liu, B.; Cheng, H. M. High-Energy MnO_2 Nanowire/Graphene and Graphene Asymmetric Electrochemical Capacitors. *ACS Nano* **2010**, *4*, 5835−5842.

(28) Peng, X. Y.; Liu, X. X.; Diamond, D.; Lau, K. T. Synthesis of Electrochemically-Reduced Graphene Oxide Film with Controllable Size and Thickness and its Use in Supercapacitor. *Carbon* **2011**, *49*, 3488−3496.

(29) Guo, H.-L.; Wang, X.-F.; Qian, Q.-Y.; Wang, F.-B.; Xia, X.-H. A Green Approach to the Synthesis of Graphene Nanosheets. *ACS Nano* **2009**, *3*, 2653−2659.

(30) Chen, S.; Zhu, J.; Wu, X.; Han, Q.; Wang, X. Graphene Oxide-MnO_2 Nanocomposites for Supercapacitors. *ACS Nano* **2010**, *4*, 2822−2830.

(31) Bernard, M. C.; Cortes, R.; Keddam, M.; Takenouti, H.; Bernard, P.; Senyarich, S. Structural Defects and Electrochemical Reactivity of β-$Ni(OH)_2$. *J. Power Sources* **1996**, *63*, 247−254.

(32) Xu, L.; Ding, Y.-S.; Chen, C.-H.; Zhao, L.; Rimkus, C.; Joesten, R.; Suib, S. L. 3D Flowerlike α-Nickel Hydroxide with Enhanced Electrochemical Activity Synthesized by Microwave-Assisted Hydrothermal Method. *Chem. Mater.* **2007**, *20*, 308−316.

(33) Kuang, D.-B.; Lei, B.-X.; Pan, Y.-P.; Yu, X.-Y.; Su, C.-Y. Fabrication of Novel Hierarchical β-$Ni(OH)_2$ and NiO Microspheres via an Easy Hydrothermal Process. *J. Phys. Chem. C* **2009**, *113*, 5508−5513.

(34) Clifford, A. F. The Prediction of Solubility Product Constants. *J. Am. Chem. Soc.* **1957**, *79*, 5404−5407.

(35) Ramarajan, D.; Sivagurunathan, P.; Yan, Q. Synthesis and Characterization of Sol-Processed α-MnO_2 Nanostructures. *Mater. Sci. Semicond. Process.* **2012**, *15*, 559−563.

(36) Yang, L.-X.; Zhu, Y.-J.; Tong, H.; Liang, Z.-H.; Wang, W.-W. Hierarchical β-$Ni(OH)_2$ and NiO Carnations Assembled from Nanosheet Building Blocks. *Cryst. Growth Des.* **2007**, *7*, 2716−2719.

(37) Yuan, C.; Zhang, X.; Su, L.; Gao, B.; Shen, L. Facile Synthesis and Self-Assembly of Hierarchical Porous NiO Nano/Micro Spherical

Superstructures for High Performance Supercapacitors. *J. Mater. Chem.* **2009**, *19*, 5772−5777.
(38) Lee, J. W.; Ko, J. M.; Kim, J.-D. Hierarchical Microspheres Based on α-Ni(OH)$_2$ Nanosheets Intercalated with Different Anions: Synthesis, Anion Exchange, and Effect of Intercalated Anions on Electrochemical Capacitance. *J. Phys. Chem. C* **2011**, *115*, 19445−19454.
(39) Tung, V. C.; Allen, M. J.; Yang, Y.; Kaner, R. B. High-Throughput Solution Processing of Large-Scale Graphene. *Nat. Nanotechnol.* **2009**, *4*, 25−29.
(40) Si, Y.; Samulski, E. T. Exfoliated Graphene Separated by Platinum Nanoparticles. *Chem. Mater.* **2008**, *20*, 6792−6797.
(41) Patil, U. M.; Gurav, K. V.; Fulari, V. J.; Lokhande, C. D.; Joo, O. S. Characterization of Honeycomb-Like "β-Ni(OH)$_2$" Thin Films Synthesized by Chemical Bath Deposition Method and Their Supercapacitor Application. *J. Power Sources* **2009**, *188*, 338−342.
(42) Toupin, M.; Brousse, T.; Belanger, D. Charge Storage Mechanism of MnO_2 Electrode Used in Aqueous Electrochemical Capacitor. *Chem. Mater.* **2004**, *16*, 3184−3190.
(43) Fan, Z.; Yan, J.; Wei, T.; Zhi, L.; Ning, G.; Li, T.; Wei, F. Asymmetric Supercapacitors Based on Graphene/MnO_2 and Activated Carbon Nanofiber Electrodes with High Power and Energy Density. *Adv. Funct. Mater.* **2011**, *21*, 2366−2375.
(44) Yu, G.; Hu, L.; Vosgueritchian, M.; Wang, H.; Xie, X.; McDonough, J. R.; Cui, X.; Cui, Y.; Bao, Z. Solution-Processed Graphene/MnO_2 Nanostructured Textiles for High-Performance Electrochemical Capacitors. *Nano Lett.* **2011**, *11*, 2905−2911.
(45) Jiang, H.; Li, C.; Sun, T.; Ma, J. High-Performance Supercapacitor Material Based on Ni(OH)$_2$ Nanowire-MnO_2 Nanoflakes Core-Shell Nanostructures. *Chem. Commun.* **2012**, *48*, 2606−2608.
(46) Kim, H.; Popov, B. N. Synthesis and Characterization of MnO_2-Based Mixed Oxides as Supercapacitors. *J. Electrochem. Soc.* **2003**, *150*, D56−D62.
(47) Chen, C.-Y.; Fan, C.-Y.; Lee, M.-T.; Chang, J.-K. Tightly Connected MnO_2-Graphene with Tunable Energy Density and Power Density for Supercapacitor Applications. *J. Mater. Chem.* **2012**, *22*, 7697−7700.
(48) Xia, X.; Tu, J.; Mai, Y.; Chen, R.; Wang, X.; Gu, C.; Zhao, X. Graphene Sheet/Porous NiO Hybrid Film for Supercapacitor Applications. *Chem.—Eur. J.* **2011**, *17*, 10898−10905.
(49) Lei, Z.; Zhang, J.; Zhao, X. S. Ultrathin MnO_2 Nanofibers Grown on Graphitic Carbon Spheres as High-Performance Asymmetric Supercapacitor Electrodes. *J. Mater. Chem.* **2012**, *22*, 153−160.
(50) Zhao, X.; Zhang, L.; Murali, S.; Stoller, M. D.; Zhang, Q.; Zhu, Y.; Ruoff, R. S. Incorporation of Manganese Dioxide within Ultraporous Activated Graphene for High-Performance Electrochemical Capacitors. *ACS Nano* **2012**, *6*, 5404−5412.
(51) Cheng, Y.; Zhang, H.; Lu, S.; Varanasi, C. V.; Liu, J. Flexible Asymmetric Supercapacitors with High Energy and High Power Density in Aqueous Electrolytes. *Nanoscale* **2013**, *5*, 1067−1073.
(52) Hu, C.-C.; Chen, J.-C.; Chang, K.-H. Cathodic Deposition of Ni(OH)$_2$ and Co(OH)$_2$ for Asymmetric Supercapacitors: Importance of the Electrochemical Reversibility of Redox Couples. *J. Power Sources* **2013**, *221*, 128−133.
(53) Tang, P.; Zhao, Y.; Xu, C. Step-by-Step Assembled Poly(3,4-ethylenedioxythiophene)/Manganese Dioxide Composite Electrodes: Tuning the Structure for High Electrochemical Performance. *Electrochim. Acta* **2013**, *89*, 300−309.
(54) Deng, L.; Hao, Z.; Wang, J.; Zhu, G.; Kang, L.; Liu, Z.-H.; Yang, Z.; Wang, Z. Preparation and Capacitance of Graphene/Multiwall Carbon Nanotubes/MnO_2 Hybrid Material for High-performance Asymmetrical Electrochemical Capacitor. *Electrochim. Acta* **2013**, *89*, 191−198.
(55) Mak, W. F.; Wee, G.; Aravindan, V.; Gupta, N.; Mhaisalkar, S. G.; Madhavi, S. High-Energy Density Asymmetric Supercapacitor Based on Electrospun Vanadium Pentoxide and Polyaniline Nanofibers in Aqueous Electrolyte. *J. Electrochem. Soc.* **2012**, *159*, A1481−A1488.